

# **CHARACTERIZATION OF INHIBITOR AND CORROSION PRODUCT FILM USING ELECTROCHEMICAL IMPEDANCE SPECTROSCOPY (EIS)**

**H. B. Wang, H. Shi, T. Hong, C. Kang and W. P. Jepson**

Corrosion center, Ohio University  
340 ½ West State Street, Athens, OH 45701

## **ABSTRACT**

In the work, EIS and Tefal techniques were used to study the corrosion inhibitor performance in multiphase flow conditions. The experimental results show that the corrosion product layer without inhibitor is non-protective at a low temperature and low pressure environment. In slug flow at a Froude number of 6, the effectiveness of the inhibitor increases with the addition of an oil phase and reaches almost 100 % for 100 ppm of inhibitor. Tafel analysis suggest that the most possible way to decrease the corrosion rates could result from the effect of blocking the active sites on the metal surface by adsorbed imidazoline molecules. From EIS, it is shown that with an increase in the inhibitor concentration, the double layer capacitance and inhibitor film capacitance decrease sharply, whilst the solution resistance in the pores increases. The analysis shows that the formation of a very dense inhibitor film on the metal surface rather than an increase in the corrosion product film thickness. This may explain both the decrease of charge transfer resistance and the decrease of film capacitance.

**Keywords:** imidazoline, anodic and cathodic reaction, slug flow, film capacitance

## INTRODUCTION

In oil and gas production industry, internal corrosion of carbon steel pipeline is a well-known phenomenon and a serious problem, and inhibition is the most cost effective and flexible method of corrosion control. Therefore, knowledge of the mechanism of a corrosion inhibition process is highly desirable in the design and proper selection of inhibitors.

Inhibitors can interfere with the anodic or cathodic reaction, and can form a protective barrier on the metal surface against corrosive agents or can work by a combination of these actions. For application in the petroleum industry, organic inhibitors containing nitrogen (amines) are often used because of their effectiveness and availability. When a corrosion inhibitor is added to a system, adsorption of inhibitor molecules at the metal-solution interface occurs and this is accompanied by a change in potential difference between the metal electrode and the solution due to the non-uniform distribution of electric charges at the interface<sup>[1]</sup>. The inhibitors efficiency depends on many factors. From a macroscopic view, it depends on flow patterns, solution chemistry, temperature, pressure, etc. At a molecular level, it depends on the number of adsorption sites, inhibitors' charge density, molecular size, mode of interaction with the metal surface, electronic structure of the molecules etc.

Many researchers have been working on the performance and mechanisms of the inhibitors based on the test results in small-scale laboratory systems. The studies of Mansfield (1985) point out that interface inhibition presumes a strong interaction between the corroding substrate and the inhibitor<sup>[2]</sup>. The two-dimensional adsorbate layer can affect the basic corrosion reactions in various ways : that caused by the geometric blocking effect of adsorbed inhibitive species on the metal surface; and that due to the effect of blocking the active sites on the metal surface by adsorbed inhibitive species; that due to the electro-catalytic effect of the inhibitor or its reaction products. For the first case, the inhibition comes from the reduction of reaction area on the surface of the corroding metal, whereas for the other two modes, the inhibition effects are due to the changes in the average activation energy barriers of the anodic and cathodic reactions of the corrosion process.

Using potential dynamic methods, Cao (1996) studied the inhibition mechanism and efficiency. The study shows that if the shift of corrosion potential due to addition of an interface inhibitor is negligible, the inhibition is most probably caused by a geometric blocking effect of the adsorbed inhibitive species on the surface of the corroding metal<sup>[3]</sup>.

The two main types of the adsorption of an organic inhibitor on a metal surface are physical or electrostatic and chemisorption. Chemisorption is the transfer, or sharing of the inhibitor molecules'

charge to the metal surface, forming a coordinate-type bond. Chemisorption is probably the most important type of interaction between the metal surface and an inhibitor molecule<sup>[11]</sup>. The studies of Wang<sup>[4]</sup> provide further information on the electron configuration of several imidazoline inhibitors by the quantum chemical calculation and the correlation between molecular structure and behavior of corrosion inhibition. It is concluded that electron donor group introduced, particularly, the substituent group with conjugated system, to imidazoline ring will improve corrosion inhibition efficiency of imidazoline derivatives. The N-C-N bond in imidazoline molecule is of p- $\pi$  conjugation property. Introduction of electron releasing substituent or conjugation system on the C atom will remarkably strengthen the chemical adsorption of the N atom on the metal surface. The XPS results<sup>[5]</sup> also show that nitrogen is clearly evident from the imidazoline-inhibited surface but was absent with the uninhibited ones. Thus, the nitrogen provides a marker for the presence of the chemical inhibitors on the iron oxide.

Many previous studies<sup>[6,7,8]</sup> pointed out that the main components of the scale are iron carbonate ( $\text{FeCO}_3$ ) and iron carbide ( $\text{Fe}_3\text{C}$ ). Like the metal,  $\text{Fe}_3\text{C}$  is an electronic conductor. The cathodic corrosion reaction, therefore, can occur as readily on  $\text{Fe}_3\text{C}$  as on the surface of the steel itself. This led to the possibility of galvanic coupling between the steel substrate and the layer or undissolved  $\text{Fe}_3\text{C}$ . In general, the presence of conductive compounds in a corrosion layer plays an essential role in their protectiveness and in the risk of uniform corrosion degenerating into localized attack. The typical corrosion product layer in an uninhibited system is on the order of microns thick and is porous<sup>[9,10]</sup>. In the presence of corrosion inhibitor, such as oleic imidazolines and phosphate esters, the inhibitor film is on a molecular level while the corrosion layer is on a microscopic order. Due to the differences in length scale, the inhibitor sees the corrosion product layer as a surface<sup>[5]</sup>. Kowata (1996) also indicates that the corrosion product layer is very porous and has enough pore size for the inhibitor to migrate<sup>[11]</sup>. Therefore, the study of inhibitor performance is always associated with the study of corrosion product film.

The understanding of  $\text{CO}_2$  corrosion inhibitors is limited in multiphase flow conditions, especially since very little is known about the inhibitor film formation mechanisms, as well as the porosity and thickness of the inhibitor film. Electrochemical impedance spectroscopy (EIS) has been used to study the corrosion product film and inhibitor performance extensively during last twenty years. Most of the works have been carried out to for the coating film system<sup>[12]</sup> and the methods used are extrapolated to study the inhibitor film<sup>[13]</sup>.

However, most works in understanding the corrosion phenomenon in oil and gas pipelines are carried out using rotating cylinder electrodes and small diameter flow loops, which do not take into account the effect of multiphase flow and the presence of various flow regimes encountered in oil-water-gas pipelines. For multiphase flow in horizontal pipelines, various flow regimes are seen, such as stratified, plug, slug and annular flow.<sup>[14,15]</sup> Slug flow regime can be found in many multiphase pipeline with associated high turbulence and bubble impact mechanism. Since the slug flow is a severe corrosion environment<sup>[16, 17]</sup>, in this work, the performance and mechanism of the inhibitor were studied using EIS and Tafel techniques at these conditions.

### **EXPERIMENTAL SETUP & PROCEDURE**

All the flow loop experiments were carried out in a I.D. 0.1016 m, 15 m long acrylic multiphase pipeline system. The schematic layout of the low pressure and low temperature system is shown in Figure 1. The CO<sub>2</sub> partial pressure was maintained at 0.136 MPa and the solution temperature was kept at 40 °C. Table 1 shows the detail information about the tests matrix.

Before each experiment, the system is de-oxygenated with carbon dioxide for 5 hours until the concentration of the dissolved oxygen in the solution is less than 10 ppb. Once the de-oxygenation process is completed, the EIS and electrical resistance (ER) probes, which are polished by 600-grit sandpaper and washed by acetone, are quickly inserted into the test section and the experiments are started. A constant pH value of 5.3 was measured during experiments since temperature and CO<sub>2</sub> partial pressure is kept constant.

The AC impedance spectra are generated by Gamry® PC4 corrosion monitoring system. The EIS measurements are carried out at open circuit potential with 4 mV AC voltage amplitude. The experimental results of the impedance were analyzed in terms of an equivalent circuit using Nonlinear Least Squares Fit Technique provided by the Gamry software. The reference and auxiliary electrodes of the EIS probe are made of 316L stainless steel, while the working electrode is made of C-1018 carbon steel with an area 0.785 cm<sup>2</sup>. The equivalent circuit typically used to describe the behavior of inhibitor or paint film was also used in this work, which is shown in Figure 2. All the capacitors were mathematically simulated using a constant phase element (CPE) in order to model the phenomena, which do not exactly behave as pure capacitors.

## RESULTS & DISCUSSION

### 100 % WATER CUT

Figure 3 shows the Nyquist plots for slug flow of Froude Number (Fr) 6 at different exposure times. It is shown in Nyquist diagram that the origin of the semi-circle locates below the real axis of impedance. This depression of the semicircle may be due to the changing of surface roughness and the effect of geometry on the current distribution, which is also observed by other researchers<sup>[13]</sup>.

The change of charge transfer resistance  $R_{ct}$  calculated from EIS plots and the corrosion rates calculated from the ER experiments at different exposure time are shown in Figures 4a and Figure 4b. The corrosion rates for slug flow at a Froude numbers of 6, 9, and 12 are 1.4, 1.5, 1.7 and 1.7 mm/y at 1, 2, 3, and 4 hours, 1.7, 1.7, 1.9, and 1.8 mm/y at 1, 2, 3, 4, 5 hours, and 2.3, 2.3 and 2.4 mm/y at 1, 2, 3 hours, respectively. From the corrosion rates values, it can be seen that the corrosion process, which includes both diffusion steps and kinetic steps, gradually becomes stable during first 3-4 hours. It is seen that corrosion rates in slug flow increase with an increase in higher Froude number. This is because, at a Froude number of 12, the corrosion environment is severe due to the high turbulent intensity and strong bubble impact<sup>[16]</sup>.

The slight decrease of  $R_{ct}$  values shown in Figure 4a is consistent with the ER results, which may indicate that micro localized corrosion is accompanying with the general corrosion process<sup>[6]</sup>. This may also suggest that little or no protective corrosion product film has been formed on the metal surface. When carbon steel is exposed, the corrosion product  $FeCO_3$  and the iron carbide ( $Fe_3C$ ) from the steel itself, may form a mixture on the metal surface<sup>[7]</sup>. The main effect of cementite is then to form additional cathodic reaction sites. The solubility of ferrous carbonate is fairly high in a  $CO_2$  containing solution with a  $HCO_3^-$  content<sup>[6]</sup>. Therefore, it is possible that most of the product of anodic reaction, ferrous ions, will dissolve in the water without forming  $FeCO_3$  scales especially at high turbulent multiphase conditions. This will then leave, at the steel surface, some uncorroded  $Fe_3C$  released from the corroded steel. This forms a conductive, porous layer on which the cathodic reaction can take place.

Another possible reason is that the size of the pores in the mixture layer is large enough for electrochemical active species to transport freely at these multiphase flow conditions. This is reasonable because of the strong impact of gas bubbles and collapse can remove the scale on the metal surface and then leave large-size pores.

Initially, imidazoline based inhibitors are used at a concentration of 50 ppm in a 100 % water cut environment. Figure 5 shows the charge transfer resistance for Froude numbers of 6, 9, and 12 at different exposure times. It can be seen that the  $R_{ct}$  at Froude number 6 is much higher than those 9 and 12. This indicates that the inhibitor is more effective at lower turbulent flow conditions. The corrosion rates obtained from the ER results are given in Figure 6. These results are consistent with the decrease in the charge transfer resistance from EIS experiments, which is inversely proportional to the corrosion rates. This also suggests that the charge transfer resistance from EIS tests could be used to study and compare the corrosion rates under different flow conditions. Both sets of results indicate that corrosion process is impeded due to the addition of the inhibitors.

The effectiveness of inhibition can be calculated by:

$$\% \text{ Effectiveness} = \frac{R_{ct,i} - R_{ct,b}}{R_{ct,i}} \times 100\% \quad (1)$$

where,  $R_{ct,i}$  is the charge transfer resistance in test with inhibitor;

$R_{ct,b}$  is the charge transfer resistance in blank test

The comparison of the inhibition effectiveness for different Froude number and different exposure time is shown in Figure 7. It is obvious that the inhibition effectiveness for Froude number 6 is much high than those for Froude number 9 and 12. There is little difference in the effectiveness at higher Froude number due to the impact of high turbulent intensity and high shear stress.

### **80 % WATER CUT**

It is noticed that, at 50 ppm of inhibitor, the readings become constant after about 5 hours. However, for 100 ppm at a Froude number of 6, there are still small changes after 7 hours. Figures 8 and 9 show the Nyquist plots and Bode plots for slug flow of Froude number 6 at 50 and 100 ppm inhibitor respectively. From the Bode plots, the phase curves become more complex with the increase of exposure time and inhibitor concentration. The change in the phase curves at high frequency would most possibly due to the formation of the inhibitor film because there are no evident phase changes at high frequency in the blank test without inhibitor.

Figure 10 shows the comparison of  $R_{ct}$  0, 25, 50 and 100 ppm of inhibitor. The most remarkable phenomenon shown in the diagrams is that the  $R_{ct}$  values of Froude 12 at 50 ppm are very low, which is only slightly higher than those at 25 ppm of Froude number 6 and 9. Further, the  $R_{ct}$  values at Froude number 6 at 100 ppm of inhibitor continuously increase during the period of exposure time, which suggest a continuous formation of inhibitor film on the metal surface due to the high bulk inhibitor concentration. The continuous formation of inhibitor film may result in both an increase of the film thickness and a decrease of the porosity. The increase of inhibitor film thickness could prevent the transportation of electrochemical active species from bulk solution to metal surface, while the increase of film coverage could decrease the number of kinetic active sites on metal surface and change the anodic or cathodic reaction energy barriers<sup>[3]</sup>.

As shown in Figure 11, all the effectiveness for 50 and 100 ppm inhibitor concentration are very high, almost reach 100 %. For the 100 % water cut, the effectiveness is not greater than 92%. Since imidazoline is oil soluble, the presence of oil phase may increase its dispersion in the solution, and then make it feasible for the adsorption of imidazoline molecules on metal surface. The corresponding ER results show that the corrosion rates are 0.3, 0.1 mm/y at 25 ppm and 50 ppm for slug flow of Froude number 6 and the corrosion rate at 100 ppm is almost zero. The comparison of charge transfer resistance between 0 and 50 or 100 ppm inhibitor concentration reveals that the inhibitor plays a very important role in hindering the corrosion process. Therefore, it is necessary to investigate the mechanism of the performance of the imidazoline based inhibitor.

### **STUDY OF INHIBITION MECHANISM**

In order to study the mechanisms of the anodic and cathodic reactions in the presence of an inhibitor, Tafel tests were carried out for slug flow at a Froude number of 6 at 80 % water cut. The potential scan range is  $\pm 10$  mV around the open circuit potential and scan rate is 0.1 mV/s. Though the scan range is small, which is within LPR techniques range in a consideration of not changing the steel surface condition, the obtained results show a Tafel curve characteristics. Figure 12 shows the Tafel curves at 0, 25, 50 and 100 ppm of inhibitor respectively, and the parameters of the analysis results are displayed at Table 2. It is clearly that the open circuit potential continuously increases from  $-515$  mV at blank test to  $-196$  mV at 100 ppm of inhibitor.

Previous studies<sup>[2,3]</sup> show that, if the shift of corrosion potential due to addition of an interface inhibitor is negligible, the inhibition is most probably caused by a geometric blocking effect of the

adsorbed inhibitive species on the surface of the corroding metal. Therefore, a possible way to decrease the corrosion is the blocking of the active sites on the metal surface by adsorbed imidazoline molecules. This may change the average activation energy barriers of the anodic and cathodic reactions and thus change the corrosion potential. This happens because the adsorption of imidazoline molecules is a chemical adsorption process, which involves the donation of a pair of electrons present on the nitrogen atom to iron metal. The N-C-N bond in imidazoline molecule is of p- $\pi$  conjugation property, which remarkably strengthen the chemical adsorption of the nitrogen atom on the metal surface<sup>[4,18]</sup>. With the decrease of open circuit potential, the corrosion current decreases sharply with the increase of inhibitor concentration. The decrease of corrosion current is directly related to the decrease of corrosion rate.

When no inhibitor is present, there is a layer of the mixture of corrosion product  $\text{FeCO}_3$  and  $\text{Fe}_3\text{C}$  on the metal surface. As discussed for 100 % water cut, this non-protective layer will form additional cathodic reaction sites and then will not decrease the overall corrosion rate. Therefore, the main function of the adsorption of imidazoline molecules is to block these active sites and change the reaction activation energy. Furthermore, the adsorbed imidazoline molecules could also form an interface geometry network above the metal surface, keeping the corrosion product  $\text{Fe}^{2+}$  and electrochemical active species  $\text{H}^+$ ,  $\text{HCO}_3^-$  and  $\text{H}_2\text{CO}_3$  from transporting to and from the metal surface and bulk solution. The accumulation of  $\text{Fe}^{2+}$  near the metal surface due to diffusion problem will increase its in situ concentration and decrease the solubility of  $\text{FeCO}_3$ . This will then cause a formation of  $\text{FeCO}_3$  in the pores and decrease the number of active sites again.

The measured cathodic and anodic reaction constants ( $\beta_a$  and  $\beta_c$ ) from the Tafel curves are round 20 mV/decade and 10 mV/decade for these tests. From following Butler-Volmer relationship<sup>[19]</sup>

$$I = I_{\text{corr}} \left\{ \exp\left[ \frac{2.3(E - E_{\text{oc}})}{\beta_a} \right] - \exp\left[ \frac{2.3(E_{\text{oc}} - E)}{\beta_c} \right] \right\} \quad (2)$$

where,  $E_{\text{oc}}$ : Open circuit potential;

$I_{\text{corr}}$ : Corrosion current;

$\beta_a$ : Anodic reaction constant

$\beta_c$ : Cathodic reaction constant



it is known that  $\beta_a$  and  $\beta_c$  are a measure of the symmetry of the activation barrier for anodic and cathodic reaction. It is observed that shape of the cathodic and anodic curves do not change much with the addition of inhibitor, i.e., the ratio of cathodic and anodic reaction constants does not change very much. This means that the inhibitor film has the same effect on the anodic and cathodic reaction. It will not only block the cathodic reaction sites but also the anodic reaction.

In present study, equivalent circuit model shown in Figures 2 is proposed to simulate the simple corrosion processes shown in Figure 13. According to previous work <sup>[12,13,20,21]</sup>, the  $R_{pf}$  in figure 2 has been interpreted as the pore solution resistance due to electrolyte penetration through the pores of inhibitor film. The capacitance  $C_{pf}$  has been interpreted as the capacitance of the dielectric inhibitor film. However, in a real system, film on the metal surface is a complex layer of both inhibitor film and corrosion product film. In this work, the film on the metal surface when inhibitor is present in solution is simply treated as inhibitor film since inhibitor molecules also treat corrosion product layer as its surface<sup>[11]</sup>. The resistance and capacitance of the porous film can be written as following<sup>[12,20]</sup>.

$$R_{pf} = \rho \frac{d}{A_{ps}} \quad (3)$$

$$C_{pf} = C_s + C_f = \epsilon_0 \epsilon_{rs} \frac{A_{ps}}{d} + \epsilon_0 \epsilon_{rf} \frac{A_{pf}}{d} = \epsilon_0 \epsilon_{rs} \frac{A_{ps}}{d} + \epsilon_0 \epsilon_{rf} \frac{A - A_{ps}}{d} \quad (4)$$

where

$C_s$  is the capacitance of solution in the pore

$C_f$  is the capacitance of inhibitor molecules

$\rho$  is the solution resistivity in the pores of the inhibitor films

$d$  is the thickness of the inhibitor films

$A_{pf}$  is the area occupied by the inhibitor film

$A_{ps}$  is the area of pores in inhibitor film

$A$  is the surface area of the EIS working electrode.

$\epsilon_0$  is the electrical permittivity of vacuum ( $8.854 \times 10^{-12}$  F/m)

$\epsilon_{rf}$  is the relative electrical permittivity of inhibitor film

$\epsilon_{rs}$  is the relative electrical permittivity of electrolyte in porous inhibitor film

Table 3 shows the simulation results for slug flow of Froude number 6 at 4<sup>th</sup> exposure time in 80 % water cut environment. As shown in the Table 3, the pore solution resistance  $R_{pf}$  which represent the diffusivity of electroactive species increase from 7 ohm to 292 ohm, which is almost 42 times higher. It is also obvious that both the double layer and inhibitor film capacitance decrease a lot with the increase of inhibitor concentration to 100 ppm.

The introduction of an inhibitor into the electric double layer changes its composition and structure<sup>[1]</sup>. The inhibitor molecules on the metal surface affect the electric double layer by causing a change in the dielectric properties of water molecules in the electric double layer. In this case, it may change the orientation of the dipoles of the water molecules which causes lowering of the dielectric constant and then decreases the double layer capacitance. The decrease of double layer capacitance may also be due to the decrease of the area where electrolyte is present due to the formation of the inhibitor film.

Equation 4 shows that the overall film capacitance is the combination of capacitance of inhibitor molecules and the solution capacitance in the pores. When more and more inhibitor molecules adsorb on the surface, it can be seen that the inhibitor film capacitance becomes much lower. The decrease of overall film capacitance may suggest that the electrical permittivity of inhibitor molecules is relatively much lower compared to the relative electrical permittivity of sea water which is about 80 (20 °C). Therefore, the decrease of the capacitance could result from both the increase of area ( $A_{pf}$ ) where inhibitor molecules adsorb on and the increase of thickness ( $d$ ) of the inhibitor film.

On the other hand, the  $R_{pf}$ , which represents the resistance of electrochemical species transporting to and from the surface and bulk solution, increase greatly from 7 ohm at 25 ppm to 292 ohm at 100 ppm. Since the  $R_{pf}$  is proportional to the thickness of the path in which electrochemical species diffuse and  $C_{pf}$  is inverse proportional to the thickness of the film, the sharp increase of the thickness of the inhibitor film is then unexpected. Thus, the decrease of the pore size due to the formation of a dense inhibitor film may explain the phenomenon. The reduction of the pore size decreases not only the overall diffusion area ( $A_s$ ) but also the conductivity of the electrochemical species in porous medium. A very dense inhibitor film will also decrease the number of the kinetic active sites where the anodic and cathodic reaction can take place, accordingly, decrease the corrosion rates.

From the above analysis, it can be concluded that the formation of a very dense inhibitor film on the metal surface can be used to explain the both the decrease of charge transfer resistance and the decrease of the electrical properties, such like the film and double layer capacitance ( $C_{dl}$  and  $C_{pf}$ ).

## CONCLUSIONS

1. For 100% water cut condition, the experimental results show that the corrosion product layer without inhibitor is non-protective at lower temperature and low pressure environment.
2. The effectiveness of the inhibitor increases with the addition of oil phase into the solution, which reaches nearly 100 % for 50 and 100 ppm concentration at slug flow of Froude number 6.
3. The open circuit potential increases with increase of inhibitor concentration in 80 % water cut flow. Tafel analysis suggest that the most possible way to decrease the corrosion rates could result from the effect of blocking the active sites on the metal surface by adsorbed imidazoline molecules.
4. With the increase of the inhibitor concentration, the double layer capacitance and inhibitor film capacitance decrease sharply, while the pore solution resistance increase evidently.
5. The analysis shows that the formation of a very dense inhibitor film on the metal surface other than the increase of film thickness could be used to explain both the decrease of charge transfer resistance and the decrease of film capacitance.
6. The information of charge transfer resistance from EIS tests which could be compared with ER results provides a very useful way to study performance of inhibitors. Other information such as film and double layer capacitance, can be used to characterize the mechanism of the inhibitor film.

## REFERENCES

1. Sastri, V. S., "Corrosion inhibitors", John Wily & Sons. Inc., 1998
2. Mansfeldm, F., Kendig, M. W. and Lorenz, W. J., 1985, " Corrosion Inhibition in Neutral, Aerated Media", J. Electronchem. Soc., Vol.132, NO.2, P290-296.
3. Cao, C., 1996, "On Electrochemical Techniques for Interface Inhibitor Research", Corrosion Science, Vol.38, No.12, pp. 2073-2082.
4. Wang D., Li Shuyuan, Y., Wang, M., Xiao, H., Chen, Z., " Theoretical and Experimental Studies of Structure and Inhibition Efficiency of Imidazoline Derivatives", Corrosion Science, Vol. 41, 1999, P1911-1919
5. Campbell, S., Jovancicevic, V., "Corrosion Inhibitor Film Formation Studied by ATR-FTIR", Corrosion/99, Paper No.484, 1999

6. Videm, K. and Kvarekvaal, J., Corrosion/96, Paper NO. 1, 1996
7. Crolet, J., Thevenot, N. and Nesic, S., Corrosion/96, Paper NO.4, 1996
8. Nesic, S., Thevenot, N., Crolet, J. and Drazic, D., Corrosion/96, Paper NO.3, 1996
9. Heuer, J.K. and Stubbins, J.F., 1998, Corrosion, 54, P566
10. Schmitt, G., Gudde, T., and Strobel-Effertz, E., "Fracture Mechanical Properties of CO<sub>2</sub> Corrosion Product Scales and Their Relation to Localized Corrosion", Corrosion/96, Paper No. 9, 1996
11. Kowata, K. and Takahashi, K., " Interaction of Corrosion Inhibitor with Corroded Steel Surface", CORROSION/96, Paper NO.219, 1996
12. Walter, G.W., 1991, Corrosion Science, Vol. 32. No.10 p1041.
13. Tan, Y.J., Bailey, S. and Kinsella, B., 1996, Corrosion Science, Vol. 38, No.9, pp 1545.
14. Dukler A. E. and Hubbard, M. G. " A model for gas-liquid slug flow in horizontal and near horizontal tubes", Ind. Engg. Chem. Found, 14, 1975, pp337-3347
15. Jepson, W. P., 1987 : " Flow characteristics in horizontal slug flow". 3 rd International conference on Multiphase Flow, The Hague, Netherlands, 18-20 May, Paper F2
16. Fan, Z., Jepson, W. P., Hanratty, T. J., International Journal Multiphase Flow, Vol. 18, No. 4, February, 1992, pp 477-484
17. Gopal, M., Jiang, L., Xie, Q.Q., Journal of Energy Resource and Technology, Vol. 120, NO.1, pp67-71, 1998
18. Hackerman N. and Hurd R. M., 1962, Proc. Int. Congress of Metallic Corrosion, London, Butterworths, P166.
19. Brett. C. and Brett, A, Electrochemistry, Oxford University Press, 1993
20. Walter, G. W., 1986, "A Review of Impedance Plot Methods Used For Corrosion Performance Ananalysis of Painted Metals", Corrosion Science, Vol. 26, No.9,pp 681-703
21. Mertens, S.F., Cooman, B.C., Temmerman, E., Corrosion, Vol. 55, NO.2, pp151-156

**TABLE 1 TEST MATRIX**

Parameter	Condition
Temperature, °C	40
CO <sub>2</sub> partial pressure, Mpa	0.136
Water cut, %	100 & 80
Inhibitor	Imidazoline based
Water	ASTM sea water
Inhibitor concentration, ppm	0, 25, 50, 100
Oil	Light hydrocarbon oil with viscosity of 2 cp at 20 °C
Flow pattern	Slug flow: Froude number 6, 9 & 12

**TABLE 2 TAFEL ANALYSIS RESULTS**

**(Slug flow of Froude number 6 at 80 % water cut environment)**

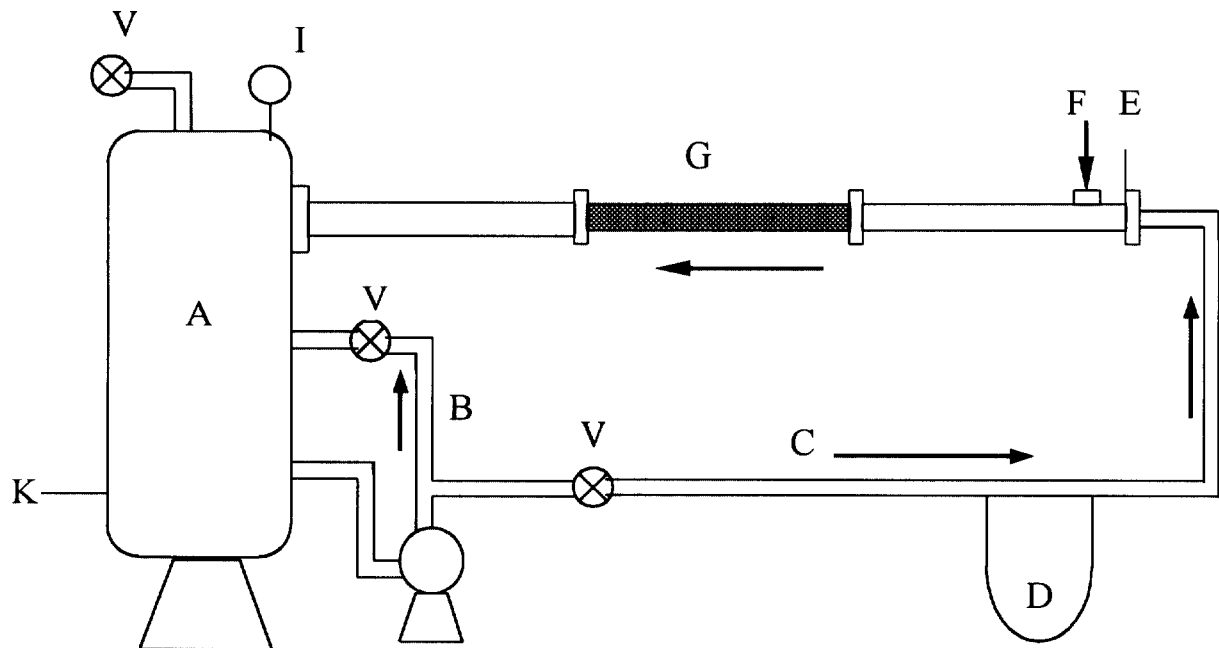
Inhibitor concentration	E <sub>oc</sub> (mV)	I <sub>corr</sub> (A/cm <sup>2</sup> )
0 ppm	-515	5.85*10 <sup>-5</sup>
25 ppm	-317	2.37*10 <sup>-5</sup>
50 ppm	-256	2.86*10 <sup>-6</sup>
100 ppm	-196	6.98*10 <sup>-8</sup>

E<sub>oc</sub>: Open circuit potential; I<sub>corr</sub>: Corrosion current; β<sub>a</sub>: Anodic reaction constant

β<sub>c</sub>: Cathodic reaction constant

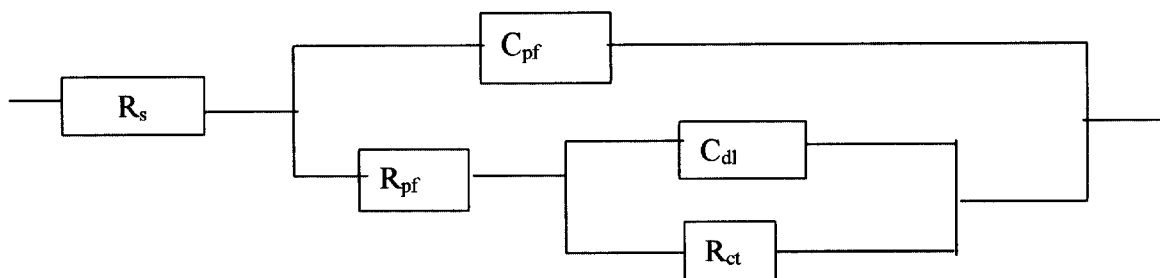
**TABLE 3 PARAMETERS OF INHIBITOR FILM AT 4<sup>TH</sup> HOUR  
FOR SLUG FLOW OF FROUDE NUMBER 6**

Concentration (ppm)	R <sub>pf</sub> (ohm)	C <sub>dl</sub> (μF)	C <sub>pf</sub> (μF)	R <sub>ct</sub> (ohm)
25	7	181	383	285
50	44	34	21	4180
100	292	28	8	6869



- |                                     |                   |
|-------------------------------------|-------------------|
| A. Liquid tank                      | G. Test section   |
| B. Bypass                           | H. Gas outlet     |
| C. Liquid feed                      | I. Pressure gauge |
| D. Orifice plate with mercury meter | K. Heater         |
| E. Flow height control gate         | V. Valves         |
| F. Gas input                        |                   |

**FIGURE 1. LAYOUT OF THE LOW PRESSURE SYSTEM**



- $C_{pf}$ : Capacitor inhibitor films  
 $C_{dl}$ : Capacitor for double layer  
 $R_s$ : Bulk solution resistance  
 $R_{pf}$ : Solution resistance in porous inhibitor film  
 $R_{ct}$ : Charge transfer resistance

**FIGURE 2 EQUIVALENT CIRCUIT MODEL**

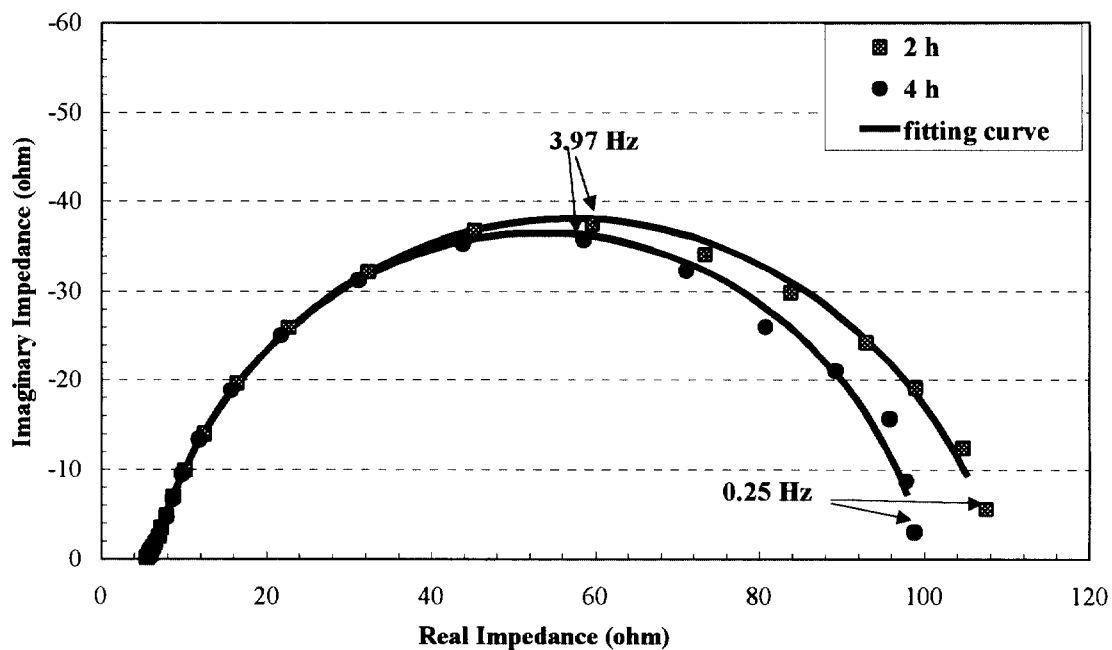


**FIGURE 3 NYQUIST PLOTS AT DIFFERENT EXPOSURE TIME**  
 (Slug flow  $Fr = 6$ , 40 C, 0.136 MPa, 100 % water cut)

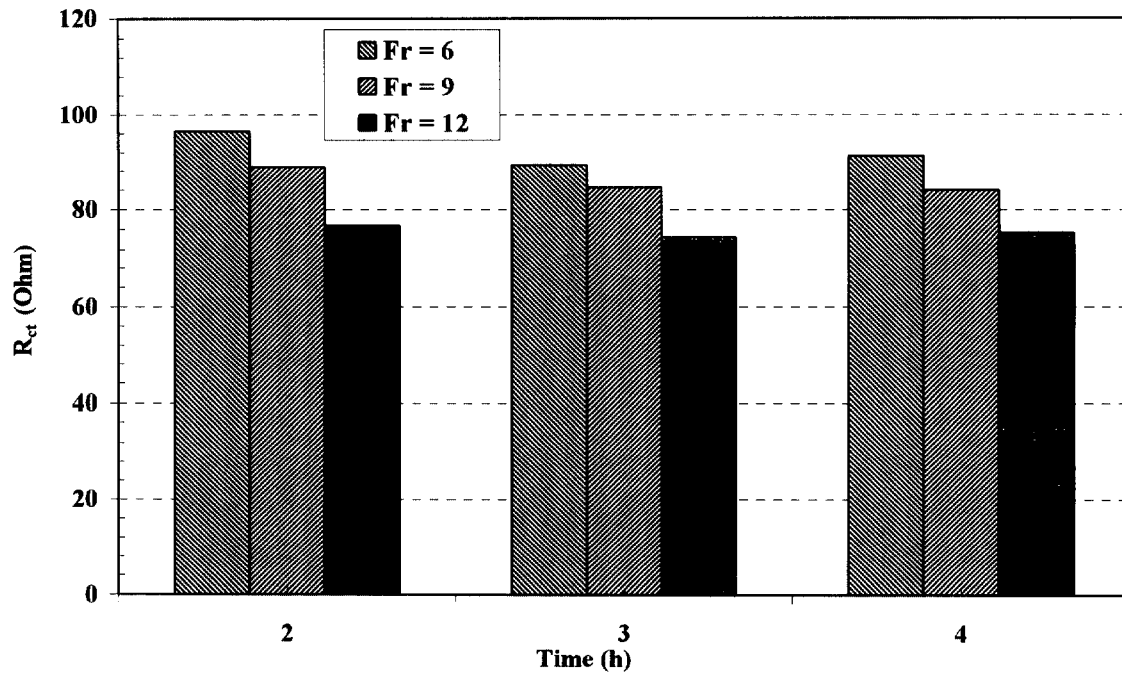


**FIGURE 4a CHARGE TRANSFER RESISTANCE AT DIFFERENT EXPOSURE TIME ( 40 C, 0.136MPa, 100 % Water cut)**

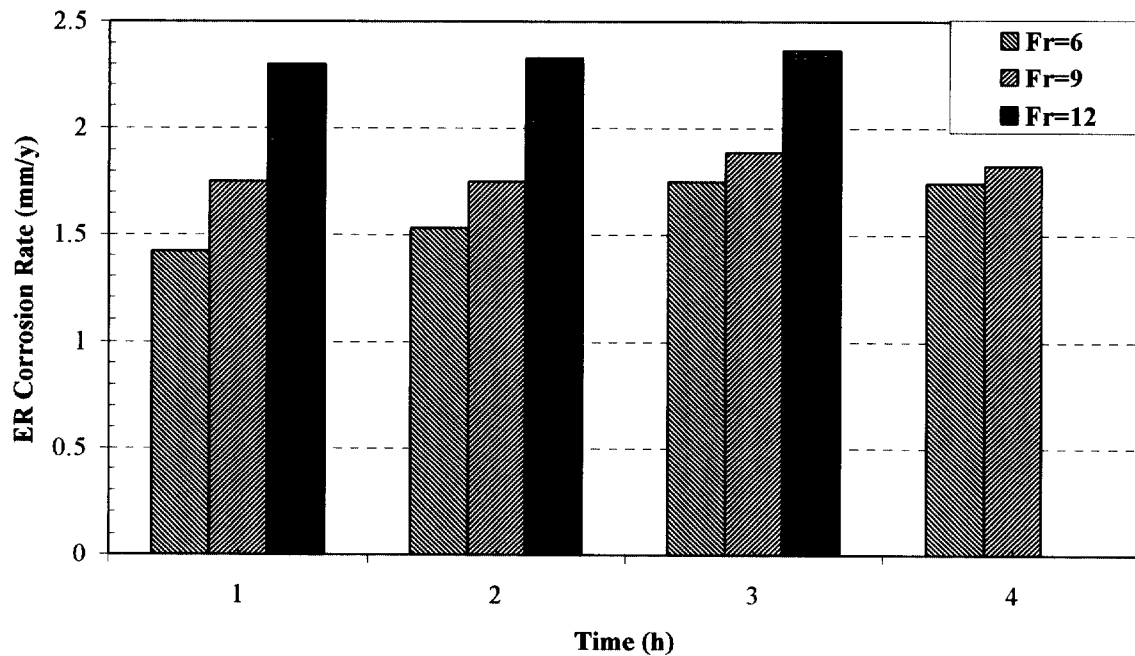


**FIGURE 4b CORROSION RATES AT DIFFERENT EXPOSURE TIME ( 40 C, 0.136MPa, 0 ppm inhibitor, 100 % water cut)**



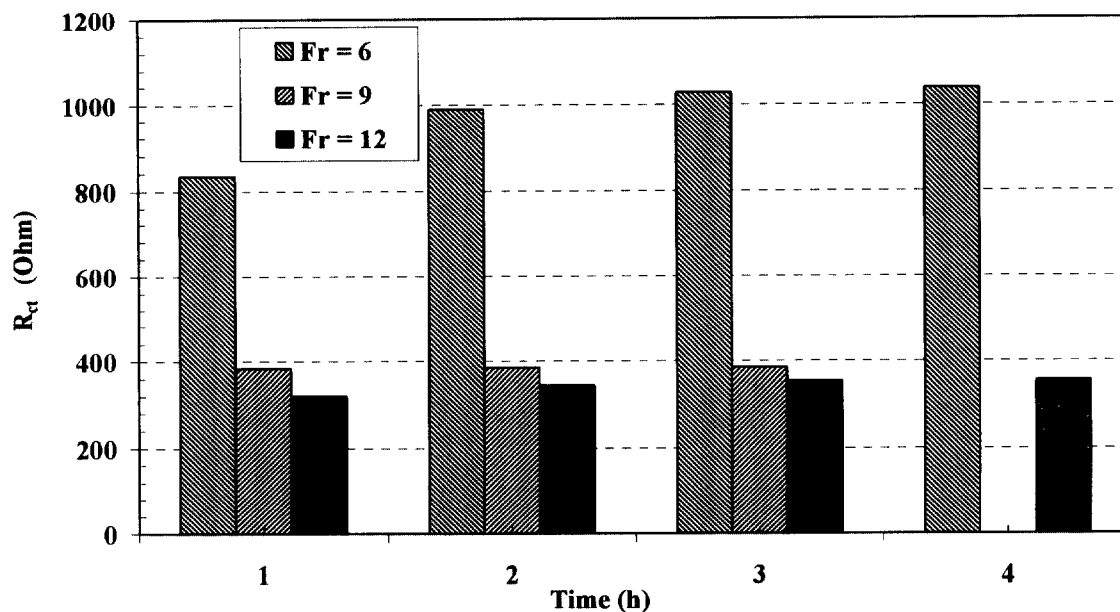


**FIGURE 5 CHARGE TRANSFER RESISTANCE AT DIFFERENT EXPOSURE TIME**  
(40 C, 0.136MPa, 100 % water cut, 50 ppm inhibitor)

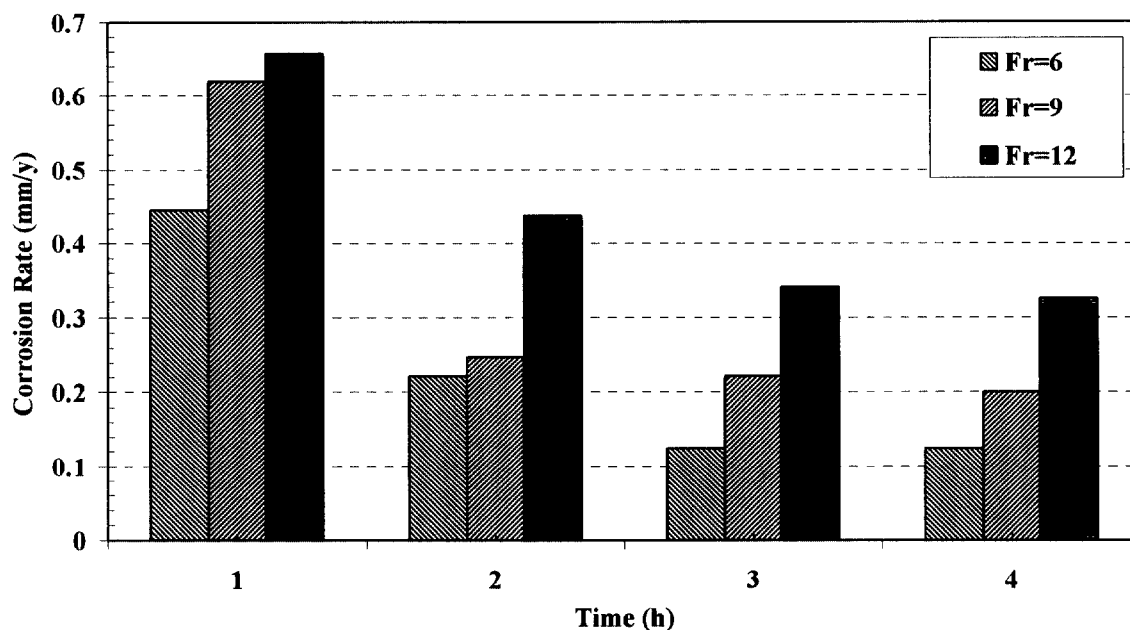


**FIGURE 6 CORROSION RATES AT DIFFERENT EXPOSURE TIME**  
(40 C, 0.136MPa, 50 ppm inhibitor, 100 % water cut)

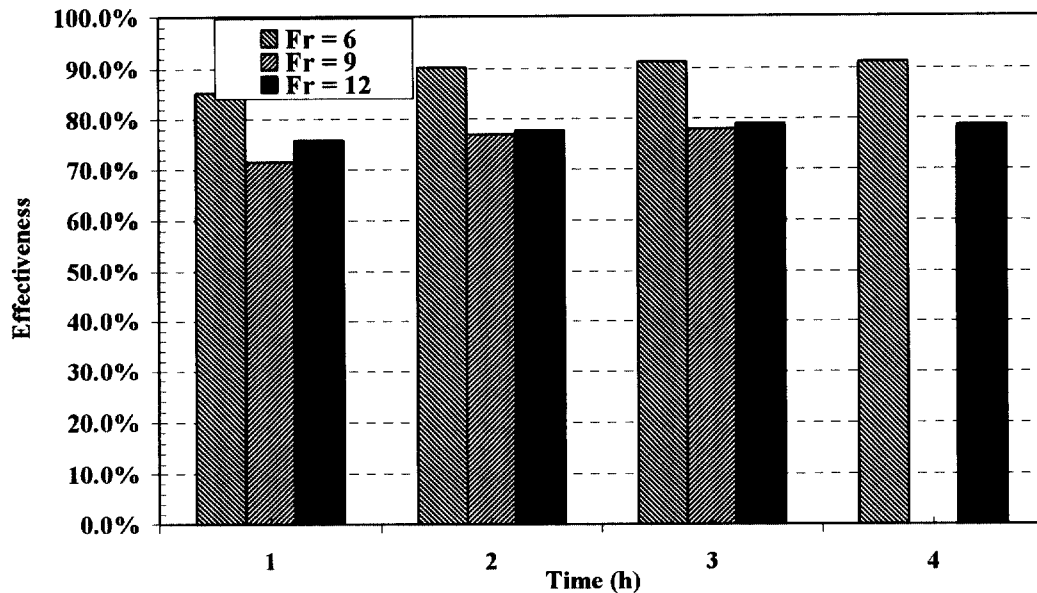


**FIGURE 7 EFFECTIVENESS OF INHIBITOR FILM AT DIFFERENT EXPOSURE TIME**  
(40 C, 0.136 MPa, 100 % water, 50 ppm)

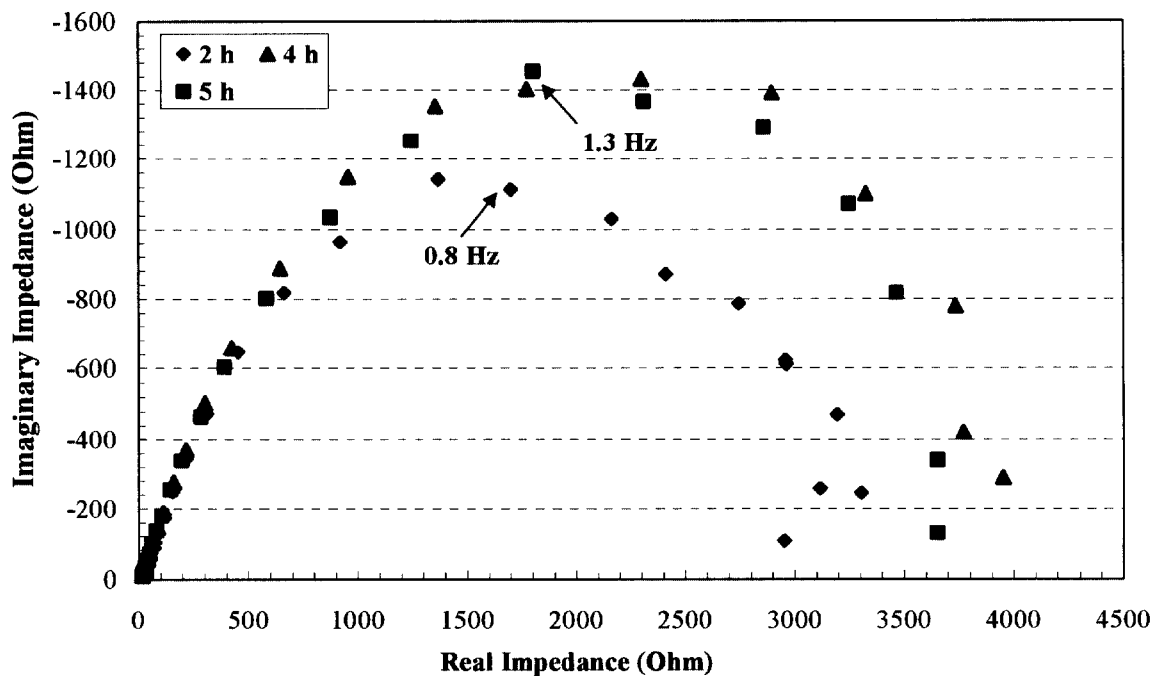


**FIGURE 8a EIS RESULTS AT DIFFERENT EXPSOURE TIME**  
(Slug flow Fr=6, 40 C, 0.136 MPa, 80 % water cut, 50 ppm inhibitor)

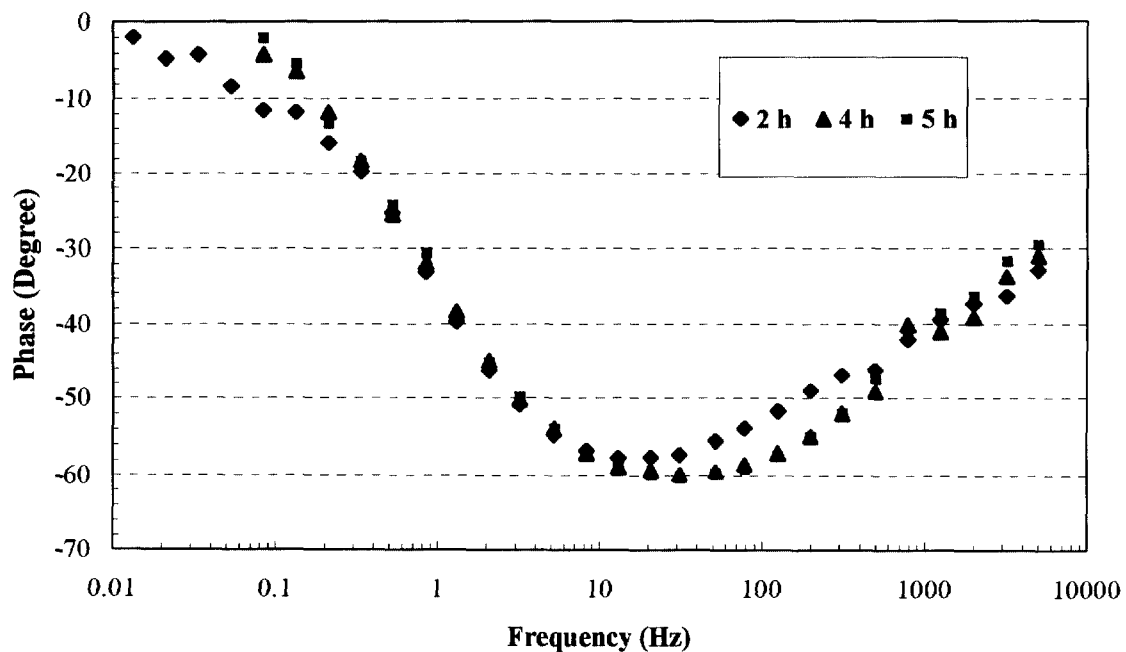


**FIGURE 8b EIS RESULTS AT DIFFERENT EXPOSURE TIMES**  
(Slug flow  $Fr=6$ , 40 C, 0.136 MPa, 80 % water cut, 50 ppm inhibitor)

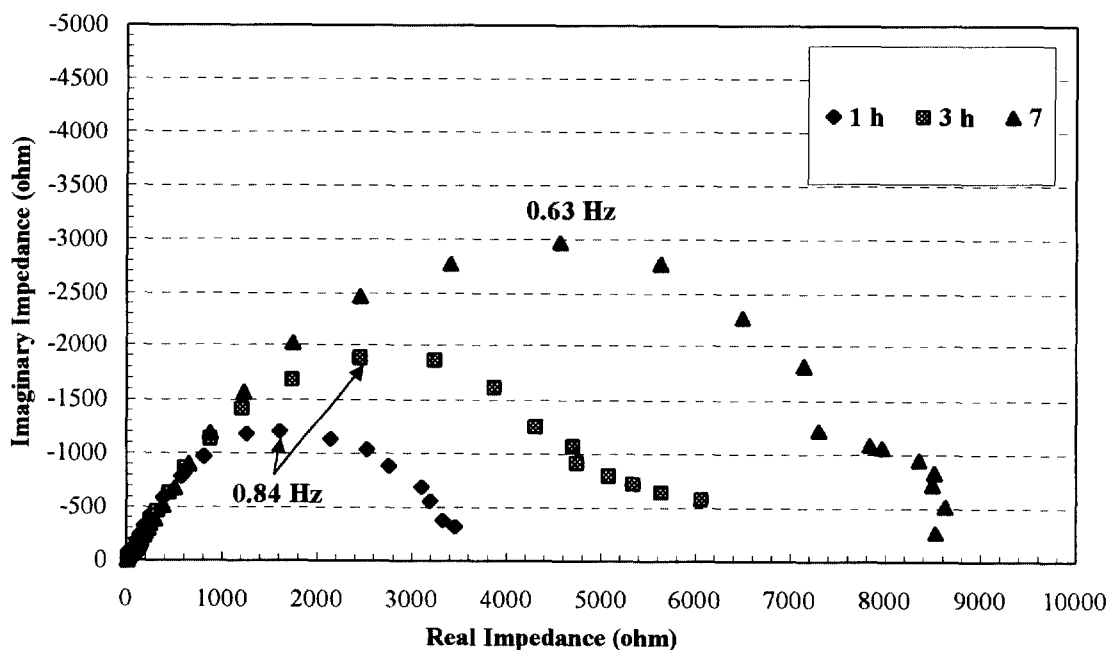


**FIGURE 9a NYQUIST PLOTS AT DIFFERENT EXPOSURE TIME**  
(Slug flow  $Fr = 6$ , 40 C, 0.136 MPa, 80 % water cut, 100 ppm)

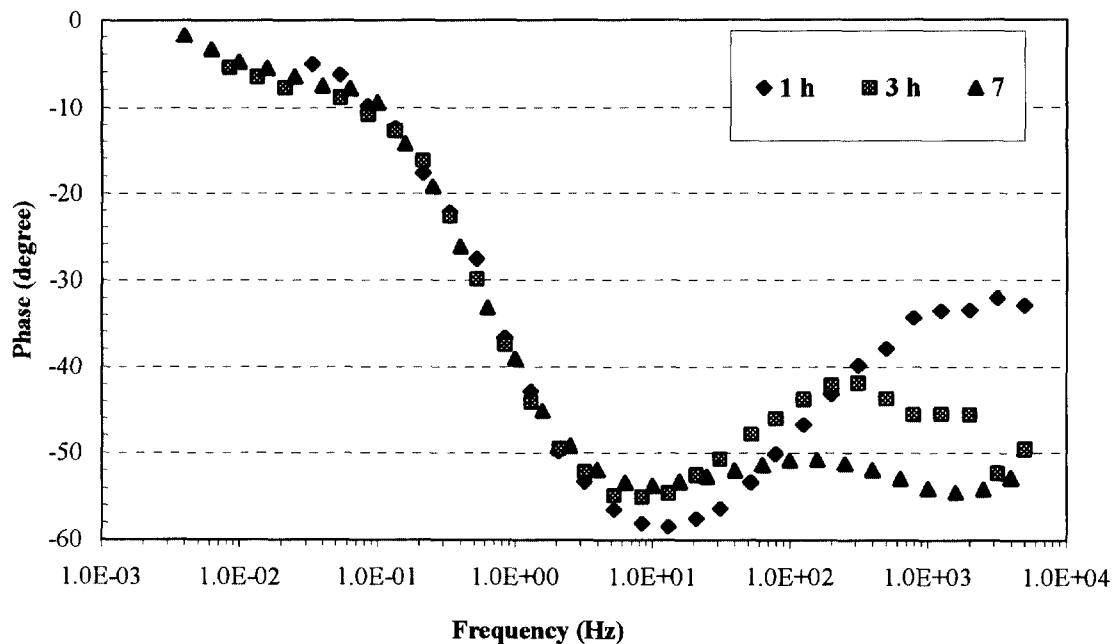


**FIGURE 9b BODE PLOTS AT DIFFERENT EXPOSURE TIME**  
(Slug flow  $Fr = 6$ , 40 C, 0.136 MPa, 80 % water cut, 100 ppm)

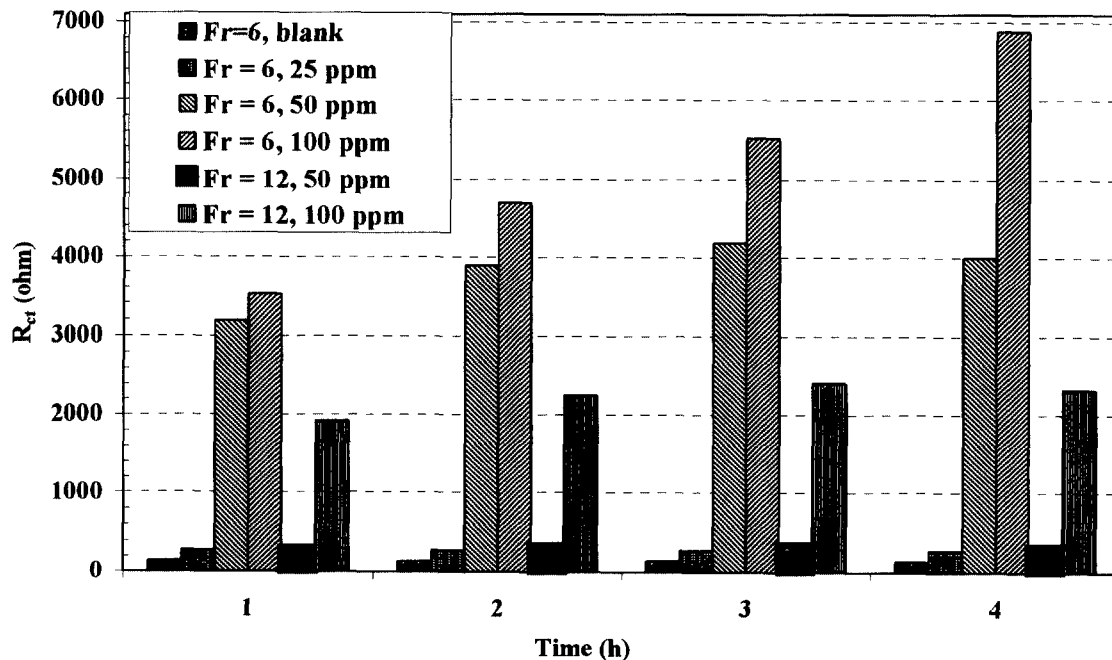


**FIGURE 10 CHARGE TRANSFER RESISTANCE AT DIFFERENT EXPOSURE TIME** (40 C, 0.136 MPa, 80 % water cut)

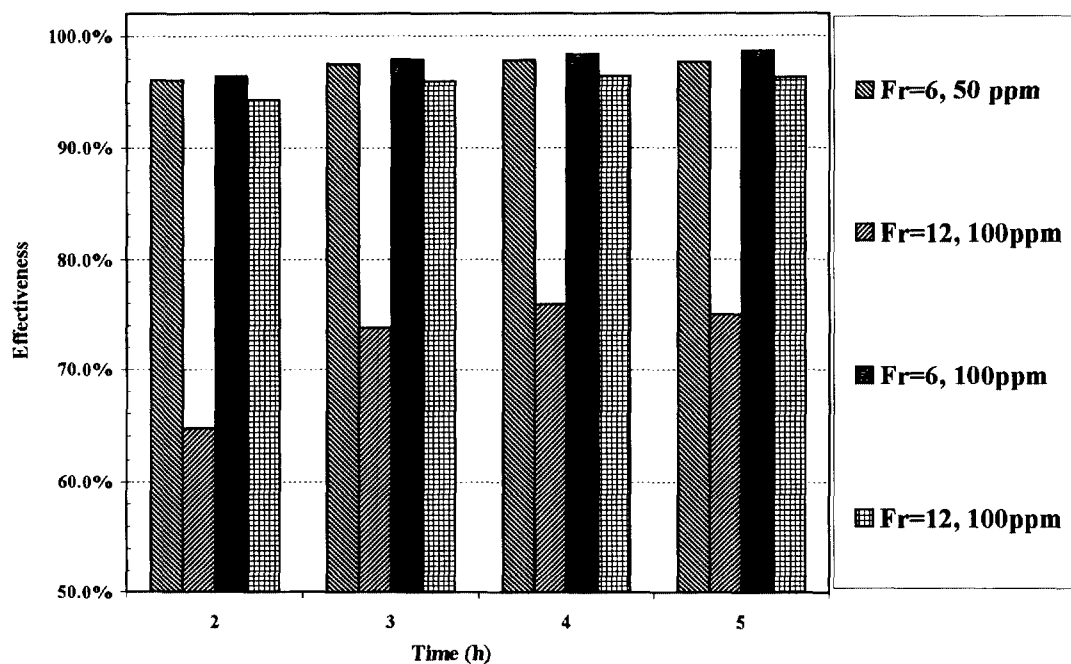


**FIGURE 11 EFFECTIVENESS OF INHIBITOR FILM AT DIFFERENT EXPOSURE TIME (Slug flow, 40 C, 0.136 MPa, 80 % water cut)**

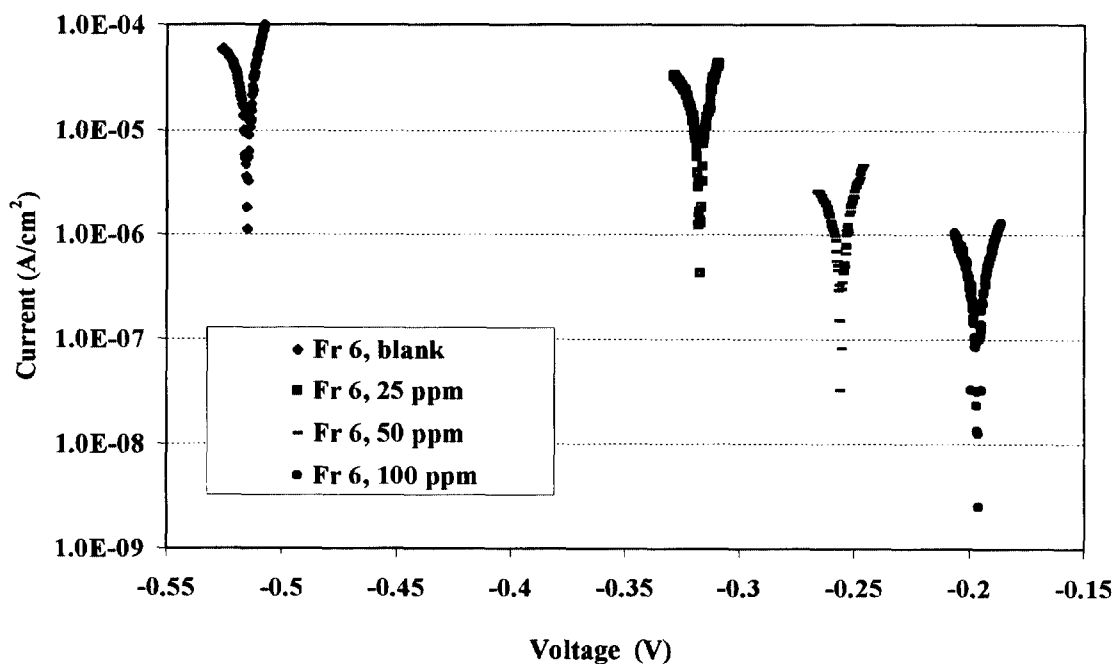


**FIGURE 12 TAFEL CURVE FOR DIFFERENT INHIBITOR CONCENTRATION (80 % water cut, Fr 6)**

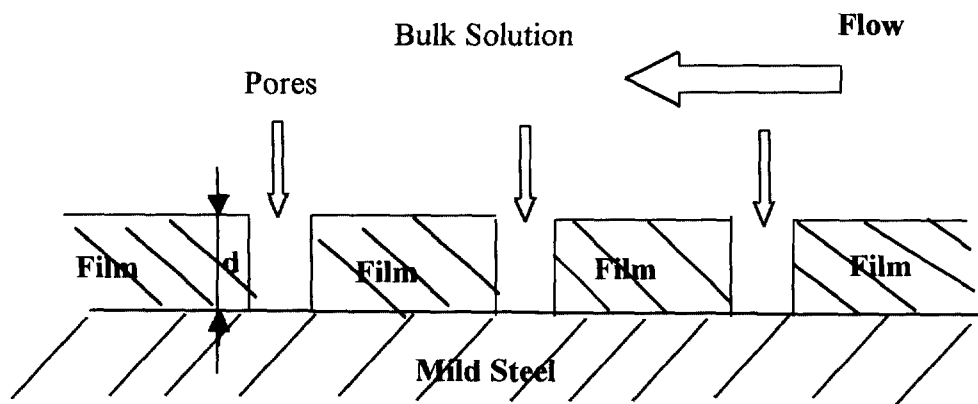


**FIGURE 13 SCHEMATIC OF A SIMPLE INHIBITOR FILM MODE**